

Geophysical Research Letters[®]

RESEARCH LETTER

10.1029/2022GL099274

Key Points:

- Observational evidence of aerosols modifying ozone profiles through their direct radiative effects
- An observation-based model disentangles the radiative effects of aerosols of different types
- Aerosol scattering augmentation effect promotes ozone formation in the upper boundary layer

Supporting Information:

Supporting Information may be found in the online version of this article.

Correspondence to:

B. Zhu,
binzhu@nuist.edu.cn

Citation:

Shi, S., Zhu, B., Tang, G., Liu, C., An, J., Liu, D., et al. (2022). Observational evidence of aerosol radiation modifying photochemical ozone profiles in the lower troposphere. *Geophysical Research Letters*, 49, e2022GL099274. <https://doi.org/10.1029/2022GL099274>

Received 25 APR 2022

Accepted 30 JUN 2022

Author Contributions:

Conceptualization: Bin Zhu

Data curation: Shuangshuang Shi, Guiqian Tang, Jiaping Xu

Formal analysis: Shuangshuang Shi

Funding acquisition: Bin Zhu, Jiaping Xu

Investigation: Cao Liu, Hong Liao, Yanlin Zhang

Methodology: Shuangshuang Shi

Project Administration: Bin Zhu

Software: Shuangshuang Shi





Validation: Guiqian Tang, Cao Liu, Junlin An, Duanyang Liu, Honghui Xu, Hong Liao, Yanlin Zhang

Writing – original draft:

Shuangshuang Shi

Writing – review & editing: Bin Zhu

Observational Evidence of Aerosol Radiation Modifying Photochemical Ozone Profiles in the Lower Troposphere

Shuangshuang Shi¹, Bin Zhu¹ , Guiqian Tang², Cao Liu¹ , Junlin An¹, Duanyang Liu³, Jiaping Xu⁴, Honghui Xu⁵, Hong Liao⁶ , and Yanlin Zhang¹ 

¹Collaborative Innovation Center on Forecast, Evaluation of Meteorological Disasters, Key Laboratory of Meteorological Disaster, Ministry of Education (KLME), Nanjing University of Information Science & Technology, Nanjing, China, ²State Key Laboratory of Atmospheric Boundary Layer Physics and Atmospheric Chemistry (LAPC), Institute of Atmospheric Physics, Chinese Academy of Sciences, Beijing, China, ³Key Laboratory of Transportation Meteorology, China Meteorological Administration, Jiangsu Institute of Meteorological Sciences, Nanjing Joint Institute for Atmospheric Sciences, Nanjing, China, ⁴Jiangsu Climate Center, Nanjing, China, ⁵Zhejiang Institute of Meteorological Sciences, Hangzhou, China, ⁶Jiangsu Key Laboratory of Atmospheric Environment Monitoring and Pollution Control, Collaborative Innovation Center of Atmospheric Environment and Equipment Technology, School of Environmental Science and Engineering, Nanjing University of Information Science & Technology, Nanjing, China

Abstract Aerosol optical effects can trigger complex changes in solar shortwave radiation (SW) in the atmosphere, resulting in significant impacts on the photochemistry and vertical structure of ozone. This paper provides observational evidence of aerosol absorbing and scattering effects on modifying the SW and ozone profiles in the low troposphere. Using field vertical measurements and observation-based model simulations, we demonstrated that absorbing aerosols decreased SW, resulting in substantial inhibition of ozone production throughout the boundary layer (BL). A similar inhibition effect occurred within the lower BL under sufficient scattering aerosols. However, the scattering augmentation effect played an additional role in enhancing the photolysis rate and promoting ozone generation in the upper BL. Hence, the observational evidence as well as our model simulations disentangled the radiative effects of different types of aerosols on the vertical structures of ozone.

Plain Language Summary Atmospheric aerosols can modify incident solar radiation by scattering and absorption, resulting in significant impacts on the photolysis rate and photochemical products in the lower troposphere. Such influences could be physically understood, but can only be observed with a detailed vertical measurement system. In this study, through vertical observational data analysis and observational constrained numerical simulations, we found that absorbing aerosols can weaken the shortwave radiation (SW) and photolysis rate in the entire layer, resulting in less ozone formation. In contrast, scattering aerosols enhance the SW and photolysis rate above the aerosol layer and promote ozone formation. Overall, the radiative effects of aerosols lead to an ozone decrease in the low layer and an increase above the boundary layer.

1. Introduction

Since 2013, elevated ambient levels of particulate matter over China have been largely alleviated by effective emission controls (Zhang et al., 2021). However, an opposite trend has been observed in the concentrations of surface ozone over China, which have rapidly increased (Li et al., 2019; Lu, Zhang, 2020). In addition to gas-phase photochemistry (Liu et al., 2021) and meteorological conditions, the photochemical production of ozone is also significantly determined by aerosol effects, for example, heterogeneous chemistry on aerosol surfaces (Li et al., 2019), vertical mixing caused by aerosol–boundary layer (BL) interactions (Gao et al., 2018), and the photolysis rate of species ($J[\text{NO}_2]$, $J[\text{O}_3/{}^1\text{D}]$, etc.) affected by aerosols via changing the intensity of solar irradiance (Dickerson et al., 1997; Li et al., 2018).

The aerosol radiative impact is a crucial factor that imposes a large constraint on chemical changes in tropospheric ozone (Zhu et al., 2021). Aerosols can be split into scattering- and absorption-dominant aerosols. Scattering-dominant aerosols (i.e., sulfate, nitrate, and organic carbon) enhance shortwave radiation (SW) in the upper part of the BL but weaken it near the surface (Liao et al., 1999), leading to an increase in the photolysis rate, acceleration of photochemical reactions, and promotion of ozone formation above the BL (Dickerson et al., 1997). Highly absorbing aerosols (i.e., black carbon (BC) and dust) reduce the ozone concentration in the

Table 1
Summary of Flights in This Study

Season	Profiles date	Profiles	Clear days	Polluted days	PM _{2.5} (μg m ⁻³)	BC (μg m ⁻³)	O ₃ (ppb)
Summer	27/05/2018–15/06/2018	113	12	4	35.6 ± 19.0	2.5 ± 1.2	73.7 ± 20.8
Winter	12/01/2019–25/01/2019	59	7	13	97.2 ± 52.3	4.0 ± 1.8	28.6 ± 14.9
Autumn	29/10/2019–09/11/2019 25/10/2020–15/11/2020	134	24	7	35.4 ± 15.3	1.5 ± 1.3	41.4 ± 18.7

Note. Values of PM_{2.5}, black carbon (BC), and ozone denote the mean concentration in the daytime at the ground.

whole troposphere due to decreasing the J[NO₂] (Gao et al., 2020). In addition, absorbing aerosols can induce heating in the upper BL and depress the vertical mixing of pollutants (Ding et al., 2016; Lu, Lu, et al., 2020), weakening the entrainment of ozone from the top of the BL to the surface in the morning (Gao et al., 2018). Many numerical studies have indicated that the decrease in the photolysis rate at the surface induced by the total extinction of aerosols weakens ozone photochemistry, reducing surface ozone by 2%–17% (Jacobson, 1998; Li et al., 2011; Maryam et al., 2021; Wang et al., 2016). For lower tropospheric ozone, the model results revealed that aerosols could result in ozone depletion near the surface and increase above the aerosol layer by altering the photolysis rate (Qu et al., 2020). However, in the lower troposphere, direct observational evidence of the effect of aerosol type on SW and photochemistry is insufficient, and the impact of aerosol type on the vertical structure of ozone remains unclear.

This study aims to characterize the impacts of aerosol of different types (absorbing and scattering) on SW and photochemistry by analyzing field vertical measurements and observational constrained model simulations. With current techniques, it is challenging to measure the vertical stratification of the radiative flux and the photolysis rates at a high spatiotemporal resolution. Therefore, this study uses several observation-based box models to bridge this research gap. The results of this study will provide a comprehensive understanding of the impacts of aerosol type on the vertical structure of ozone and contribute to the mitigation of ozone pollution in China.

2. Measurements and Methods

2.1. Observational Site and Measurements

The observation site (32.35°N, 118.72°E) was built in the Intelligent Manufacturing Industrial Park (Zhongshan Park) in the northern suburban area of Nanjing, a space for the research and design of high-tech products that directly emit light. Large farmland areas are approximately 1 km north of the site and the road transportation hub is 2.5 km northeast. The geographic location is shown in Figure S1 in Supporting Information S1. An unmanned aerial vehicle (UAV) observation platform—including a particulate matter detector (PDR-1500, TSI, USA), micro-aethalometer (microAeth AE-51, Aethlabs, USA), pyranometer (CMP21 and CUV5, Kipp & Zonen Company, Netherlands), Volatile Organic Compound sampling devices, and ozone sonde (Nanjing Junquan Science and Technology Ltd, China)—was used to obtain the datasets. To probe the effects of aerosols on SW and the vertical distribution of ozone, four UAV campaigns for vertical profiles of associated pollutants (e.g., PM_{2.5}, BC, ozone, VOCs, etc.), solar downward SW, and meteorological variables were conducted from 2018 to 2020. A detailed description of these instruments is provided in Text S1.2. Sampling flights were scheduled every 3 hr between 08:00 and 20:00 local time (LT) from the ground to a maximum height of 1 km at a speed of 3 m s⁻¹. Instruments for measuring PM_{2.5}, BC, ozone, and VOCs were mounted below the UAV, and all instrument inlets were placed 20 cm below the drone blade to minimize the influence of airflow, as suggested by Villa et al. (2016).

Table 1 summarizes the information obtained from the four field campaigns, including the time of observations, number of profiles, number of clear and polluted days, and mean concentrations of PM_{2.5}, BC, and ozone in the daytime at the ground. In the summer, winter, and autumn, 20-, 14-, and 34-day field campaigns were carried out, respectively, obtaining 113, 59, and 134 profiles. The average profiles of PM_{2.5}, BC, ozone, and VOCs for each season are shown in Figure S2 of Supporting Information S1. Days with a mean surface PM_{2.5} concentration above 45 μg m⁻³ in daytime were considered polluted days; otherwise, they were considered clean days. Winter is the season with the most severe air pollution in China owing to enhanced emissions and unfavorable meteorological conditions. Indeed, in winter, there were 13 polluted days, which was significantly more than the numbers in

summer (4 days) and autumn (7 days), despite the shorter field campaign. In winter, the mean $PM_{2.5}$ and BC mass concentrations were $97.2 \mu\text{g m}^{-3}$ and $4.0 \mu\text{g m}^{-3}$, respectively, higher than those in summer (35.6 and $2.5 \mu\text{g m}^{-3}$, respectively) and autumn (35.4 and $1.5 \mu\text{g m}^{-3}$). Ozone, a photochemical product, had a higher concentration in the summer (73.7 ppb), mainly because of stronger solar radiation and higher temperature. In this study, days in the observational period were classified into clear and cloudy days based on the Himawari-8 satellite nephograms (Lei et al., 2020). Overall, there were 43 clear days, 17 of which were polluted.

2.2. Observation-Based Models and Methods

To calculate the aerosol optical parameters, we utilized the actual vertical profiles of $PM_{2.5}$ —containing the primary and secondary aerosols in the air—and BC mass concentration and the Optical Properties of Aerosols and Clouds model (OPAC). Black carbon was assumed to be the main absorbing component among $PM_{2.5}$ and that the contribution of coarse particles was negligible owing to the absence of dust events during the field campaigns. The remaining $PM_{2.5}$ ($PM_{2.5}$ -BC) was considered as the scattering-only component. Subsequently, the modeled aerosol optical parameters at each layer were used for downstream models, such as the Santa Barbara DISORT Atmospheric Radiative Transfer (SBDART), Tropospheric Ultraviolet and Visible radiation (TUV), and the National Center for Atmospheric Research Master Mechanism to obtain the radiative fluxes, photolysis rate of NO_2 ($J[NO_2]$), and ozone changes, respectively. Detailed model introductions and configurations are given in Text S2 and Table S1 of Supporting Information S1. Four control and sensitivity experiments were designed: (a) all aerosol compositions (EXP_WA), (b) aerosol compositions other than BC (EXP_WAexBC), (c) with only BC (EXP_WBC), and (d) without aerosols (EXP_WoA). By comparing the results of the four experiments, we can quantitatively probe the effects of aerosol types on vertical structure of ozone by influencing the radiative transfer and photolysis rate. The average profile and standard deviations of 35 pairs of observed and simulated downward SW are shown in Figure S4 of Supporting Information S1. The simulations agreed well with the observations, indicating the satisfactory performance of the models.

3. Results

3.1. Observational Evidence

Figure 1 shows the relationships between ozone and BC (absorbing aerosol) and $PM_{2.5}$ -BC (scattering aerosols) over the observational period. The daytime concentrations (09:00–17:00 LT) were selected to exclude the impact of nitric oxide (NO) titration on ozone production. The BC and surface ozone had negative correlations during both cloudy (Figure 1a) and clear days (Figure 1b), indicating that the absorbing particles weakened ozone generation and accumulation. Under cloudy conditions, there was a negative correlation between $PM_{2.5}$ -BC and ozone (Figure 1a). However, the correlation between $PM_{2.5}$ -BC and ozone on clear days is less significant (Figure 1b). The difference in the relationships between $PM_{2.5}$ -BC and ozone on cloudy and clear days might indicate the obvious effect of heterogeneous reactions on ozone reduction under high-humidity conditions. Macintyre and Evans (2011) summarized a series of laboratory experiments and proposed a parameterization, based on which we estimated that the uptake coefficients of radicals and gas species (HO_2 , N_2O_5 , etc.) on the surface of aerosols were nearly two times higher on cloudy days (higher relative humidity) than on clear days. On clear days, the non-significant relationship between $PM_{2.5}$ -BC and ozone may be caused by the offset effects of aerosol extinction and scattering augmentation under strong incident radiation (Tie et al., 2005).

In the lower troposphere (below 450 m, e.g., at the surface), BC and ozone had a negative correlation. However, there was no significant correlation above 450 m in all scenarios (cloudy and clear, stable, and unstable in Figures 1c and 1e), which is attributed to the obvious light absorption by the higher BC in the lower BL. At the surface, Figure 1d shows a consistent negative correlation between ozone and $PM_{2.5}$ -BC below 800 m on cloudy days, which is very different from clear days when ozone and $PM_{2.5}$ -BC had significant positive correlations above 300 m. In the following analysis, we excluded the potential heterogeneous chemistry occurring on cloudy days and focused on the impact of aerosol radiation on the photochemical ozone profiles on clear days. Moreover, the VOCs to NO_x ratios in the lower troposphere were higher than 8 (Figure S3 in Supporting Information S1), indicating ozone formation in the ambient air was mostly NO_x limited (Seinfeld, 1989), with seldom possibility of the impact of NO titration on ozone production in the BL. Therefore, on clear days, the correlations between ozone and $PM_{2.5}$ -BC change from negative at the surface to positive above 300 m, and this could be caused by

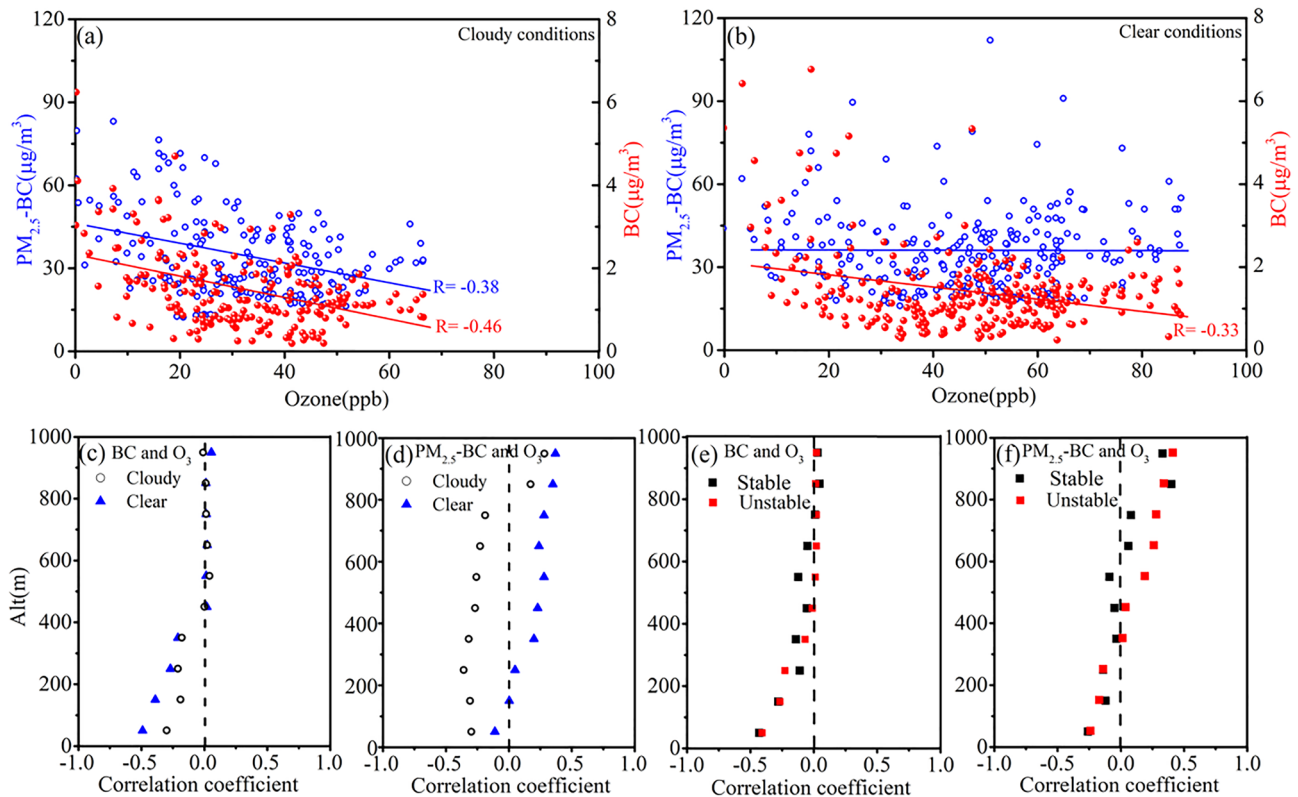


Figure 1. Relationships of surface ozone concentrations (hourly) with $PM_{2.5}$ -BC and black carbon (BC) from 09:00–17:00 LT on (a) cloudy and (b) clear days. Vertical distribution of correlation coefficient between ozone concentration and (c) BC and (d) $PM_{2.5}$ -BC on cloudy and clear days in the lower troposphere. Vertical distribution of correlation coefficient between ozone concentration and (e) BC and (f) $PM_{2.5}$ -BC on stable and unstable days.

the scattering augmentation effect of $PM_{2.5}$ -BC, which increases the photolysis rates and ozone production to overcome the effects of aerosol extinction (Li et al., 2011).

We analyzed the correlation between $PM_{2.5}$ -BC and ozone under stable (bulk Richardson number $Ri_b > 0.25$) and unstable conditions ($Ri_b < 0.25$) (Figure 1f), and positive correlations are noticed above and in the upper part of the aerosol layer in both scenarios, indicating that turbulent exchange does not impact this relationship.

Aerosols can directly influence the amount of SW, thus changing photochemical reactions (Zhang et al., 2018). Figure 2 shows the effects of $PM_{2.5}$ on observational ozone and downward SW (SWdown) profiles. The ozone, $PM_{2.5}$, and SWdown profiles were relatively homogeneous on clean days (Figure 2a), but there were sharp changes above 600 m on polluted days. To directly perceive the impacts of aerosol radiation on ozone, the vertical gradients are shown in Figures 2c and 2d. Similar to the vertical profiles in Figure 2a, the gradients varied insignificantly throughout the lower troposphere on clean days, with mean values of 8.5 W m^{-2} and $1.4 \text{ ppb ozone per hundred meters}$. There were obvious gradients at the top of BL, reaching 20.6 W m^{-2} and $4.8 \text{ ppb ozone per hundred meters}$ on polluted days. A detailed description of the positive impact of $PM_{2.5}$ loadings (under three levels of $PM_{2.5}$) on the vertical gradients of ozone and SWdown are presented in Figure S5 of Supporting Information S1, inferring that the scattering augmentation effect greatly accelerated photochemical ozone production in the upper part of the aerosol layer.

3.2. Observation-Based Simulations

The changes in upward shortwave radiation (SWup) induced by absorbing and scattering aerosols were simulated using the SBDART and are shown in Figure 3. Absorbing aerosol weakened SWup throughout the BL, especially on polluted days, reaching -3.7 W m^{-2} near the surface and -2.2 W m^{-2} at 900 m. The significant attenuation of SWup contributed to a reduction in ozone production. Under clean conditions, scattering aerosols slightly

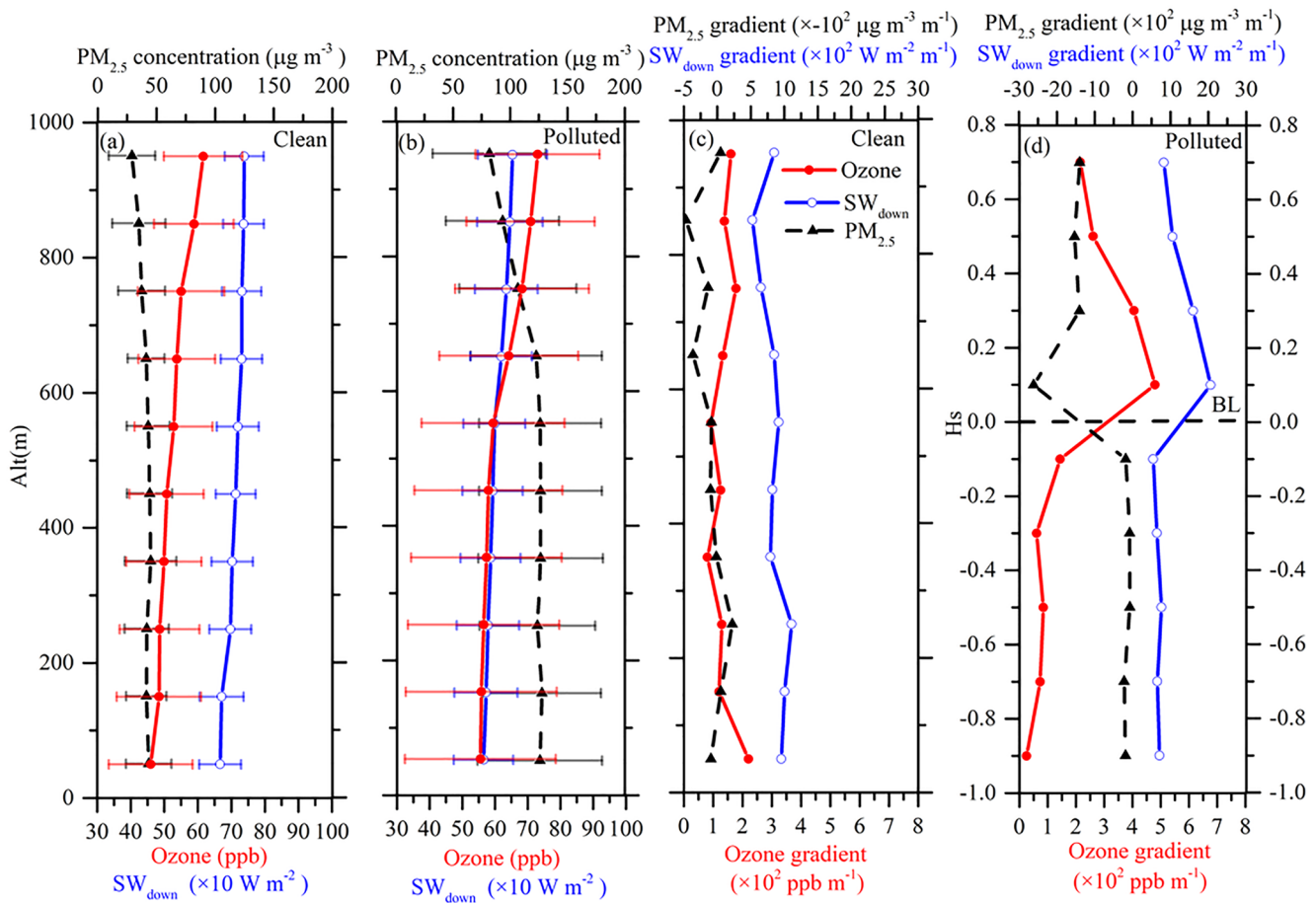


Figure 2. Vertical profiles and gradients of $PM_{2.5}$ (black dashed line), ozone (red line) and observed downward shortwave radiation (blue line) on (a and c) clean and (b and d) polluted days. The whiskers show the standard deviation. The ordinates of (a–c) denote the observed altitude. The ordinates of (d) are expressed in standard height (Hs). Hs values are assumed to be -1 and 1 at the ground and at twice the height of the boundary layer (BL), and a value of 0 is assumed at the top of BL. The black horizontal dashed line is the position of the BL.

enhanced SWup by $0.8\text{--}2.0\text{ W m}^{-2}$ below 900 m . In contrast, in the lower troposphere (below 450 m), on polluted days, scattering aerosols weakened SWup (-2.8 W m^{-2}), but a remarkable enhancement was detected above 450 m (3.6 W m^{-2}) due to enhanced scattering radiation by high $PM_{2.5}$ -BC beneath 450 m , which is close to the simulated result of Qu et al. (2020). The effects of aerosol types on radiation in each season are also essentially similar, except for some minor differences in details (Figure S6 in Supporting Information S1).

To demonstrate the impact of aerosols on $J[NO_2]$ in the actual atmosphere, we simulated $J[NO_2]$ using the observed absorbing (BC) and scattering aerosols ($PM_{2.5}$ -BC) under polluted and clean conditions at noon (12:00 LT). It is worth noting that the calculations were made under clear-sky conditions to eliminate the effects of cloud on $J[NO_2]$. The effects of aerosol type on $J[NO_2]$ can be illustrated by comparing the results of the four sets of experiments. Under clean conditions (Figure 4a), the BC and $PM_{2.5}$ concentrations were at lower levels in Nanjing (~ 1.4 and $30\text{ }\mu g m^{-3}$, respectively) than under polluted conditions and did not influence $J[NO_2]$ obviously, with a reduction of 4% at the surface. Consequently, the $J[NO_2]$ profiles did not show significant differences in the vertical direction. Under air pollution episodes (Figure 4b), BC and $PM_{2.5}$ concentrations were at relatively high levels under 600 m (~ 4.2 and $102.3\text{ }\mu g m^{-3}$, respectively) and were distributed uniformly, but dropped sharply above 600 m . As a result of the reduced radiation caused by absorbing aerosols, $J[NO_2]$ decreased with height. Similar to absorbing aerosols, scattering aerosols accumulated in the lower layer weakened the SW near the surface, which resulted in a decrease in $J[NO_2]$ in the lower layer, but the scattering augments effect led to a higher $J[NO_2]$ above 500 m . Dickerson et al. (1997) investigated the similar impacts of aerosol absorption and scattering capability on $J[NO_2]$ by simulating different aerosol property scenarios.

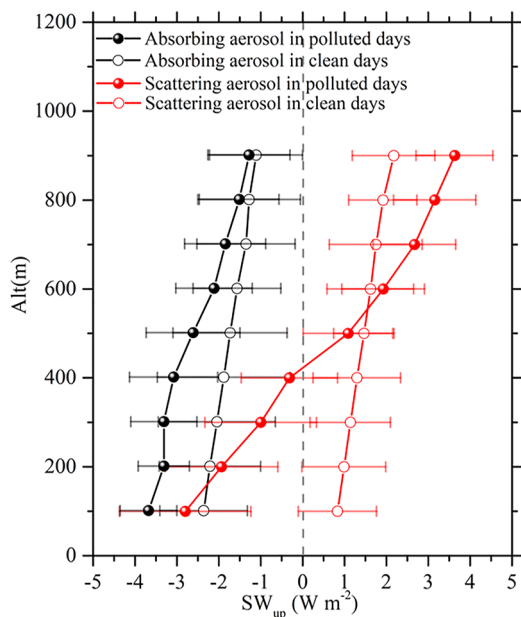


Figure 3. Influences of absorbing and scattering aerosols on the changes of upward shortwave radiation (SWup) simulated by Santa Barbara DISORT Atmospheric Radiative Transfer on polluted and clean days. Black and red lines denote the changes of SWup induced by absorbing and scattering aerosols. Solid and hollow circles are for polluted and clean days, respectively. The whiskers show the standard deviation.

Aerosol-induced changes in SW and $J[\text{NO}_2]$ can lead to changes in ozone production at different altitudes. Figure 5 displays the changes in ozone concentration and generation rate, as well as the corresponding aerosol, and observed and simulated ozone concentrations in the afternoon (14:00 LT), under clean (2020/11/11) and polluted (2020/11/07) case. The simulated ozone concentration showed a slightly larger gradient than those in the observations, which may be because diffusion and transport were not considered in the model. In the clean case, there was no significant change in the ozone concentration and generation rate owing to the homogeneous distribution of aerosols in the lower troposphere. The inhibiting effect of absorbing aerosol plays a dominant role, leading to ozone reduction of approximately 2.0 ppb at the surface and 0.5 ppb at 1,000 m. In the polluted case, absorbing aerosol reduced the ozone concentration by about 3.9 ppb at the surface and 0.6 ppb at 1,000 m. Differently, below the aerosol layer (500 m), scattering aerosols weakened ozone formation, resulting in a reduction of 1.0 ppb but a significant increase of 3.4 ppb above the aerosol layer. The combined effects (red lines) of the two types of aerosols showed that ozone reduction was greatest near the surface (4.9 ppb), which is close to the simulated results of Li et al. (2018) (5 ppb). Above 600 m, ozone increased with height, increasing by 2.8 ppb at 1,000 m, which was mainly attributed to the scattering enhancement effect induced by scattering aerosols in the BL. A sufficient number of scattering aerosols in the lower layer stimulated ozone formation in the upper part of the aerosol layer. We further examined the impacts of different ratios of BC to $\text{PM}_{2.5}$ (i.e., 1%, 5%, and 10%) on $J[\text{NO}_2]$ and ozone vertical profiles (Figure S7 in Supporting Information S1). There is no essential change in the

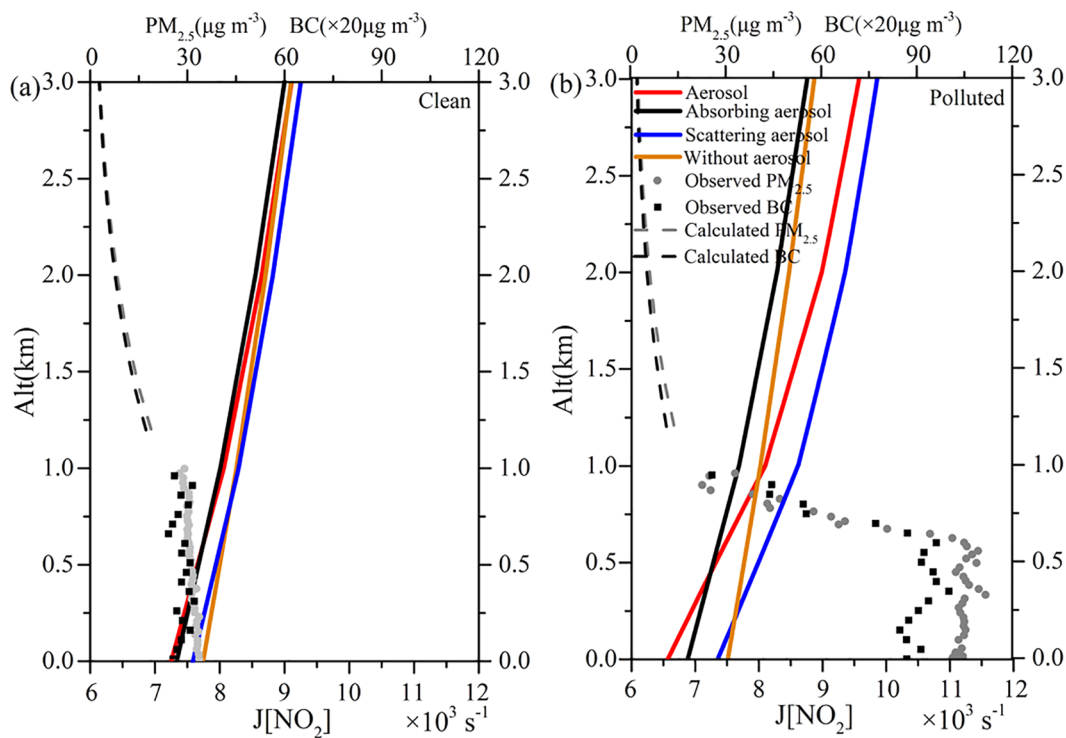


Figure 4. Profiles of $J[\text{NO}_2]$ of different aerosol types and mass concentration of $\text{PM}_{2.5}$ and black carbon (BC) on (a) clean and (b) polluted days. Red, black, blue, and brown solid lines are the simulated $J[\text{NO}_2]$ for EXP_WA, EXP_WBC, EXP_WAexBC, and EXP_WoA, respectively. Black squares and gray dots denote the observed BC and $\text{PM}_{2.5}$ mass concentrations. Black and gray dashed lines denote the derived BC and $\text{PM}_{2.5}$ mass concentrations, respectively.

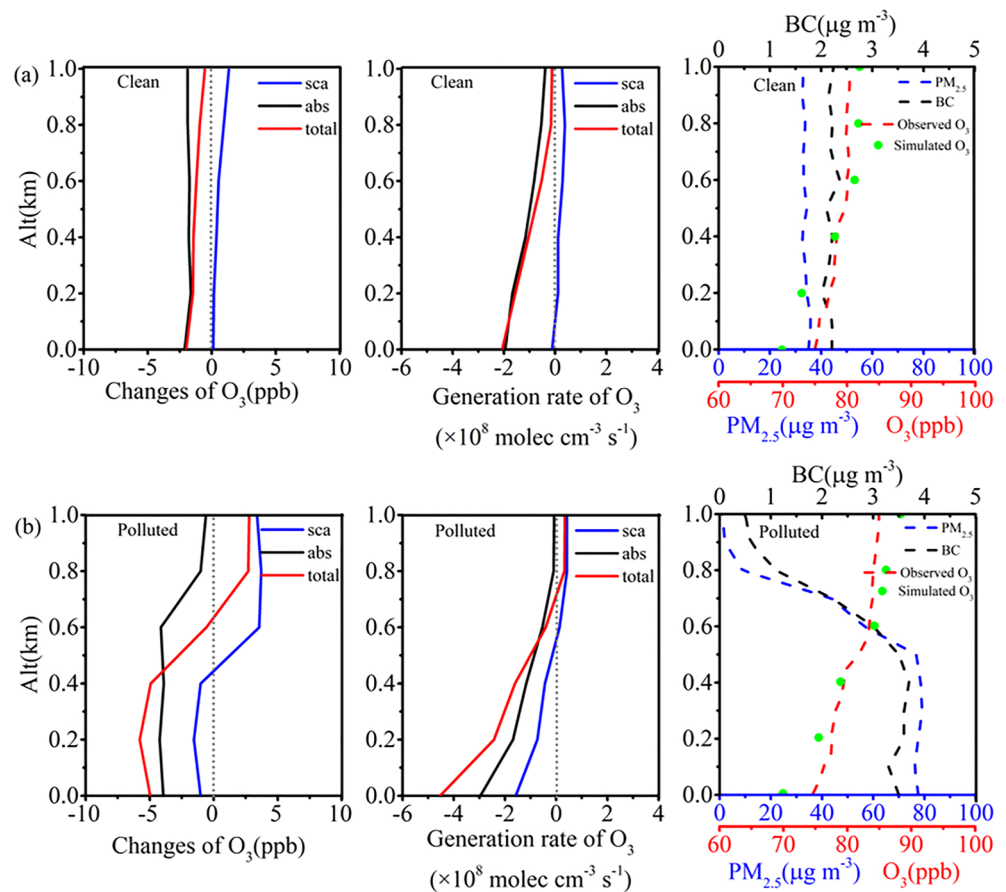


Figure 5. Changes in ozone concentration, ozone generation rate, and aerosol concentrations in the afternoon (14:00 LT) on a (a) clean day (2020/11/11) and (b) polluted day (2020/11/07). Blue, black, and red lines represent the influences of scattering, absorbing, and total aerosols on ozone concentrations and ozone generation rates, respectively. Blue, black, and red dashed lines denote the observed $PM_{2.5}$, BC, and ozone concentration. Green dots denote the simulated ozone concentration.

effect of aerosol radiation on the vertical structures of ozone, but the increased proportions of BC result in greater inhibition of ozone formation.

4. Conclusion and Discussion

Tropospheric aerosols impose constraints on photochemical reactions and their products. Based on field vertical measurements, we revealed the phenomenon that absorbing aerosol (BC) and ozone were always negatively correlated in the lower BL, but scattering aerosols ($PM_{2.5}$ -BC) and ozone had significant positive correlations in the upper layer. Higher aerosol loading within the BL played an additional role in enhancing the SW above the BL and greatly accelerating the photochemical ozone production therein.

Observational constrained models were utilized to disentangle the radiative effects of aerosols of different types on $J[NO_2]$ and ozone vertical profiles. We demonstrated that absorbing aerosols decreased SWup and weakened ozone photochemical generation throughout the entire BL. A similar inhibition effect occurred within the lowest several hundred meters of the BL under sufficient scattering aerosols. In contrast, scattering aerosols enhanced SWup and $J[NO_2]$, consequently promoting ozone generation in the upper BL.

It should be noted that the potential effects of heterogeneous chemistry and turbulent exchange are certainly important in lower tropospheric ozone production and depletion. In this study, observational and modeling results mainly focused on isolated radiative impacts and demonstrated that scattering augments the effect on ozone production in the upper part of the aerosol layer.

Data Availability Statement

The observational and data are placed in <http://doi.org/10.5281/zenodo.6802555>. The MEIC emission inventory are available from <http://meicmodel.org>. The surface albedo data are available from https://ladsweb.modaps.eosdis.nasa.gov/archive/allData/61/MYD05_L2/. The water vapor data are available from <https://ladsweb.modaps.eosdis.nasa.gov/archive/allData/6/MCD43A3/>. The ozone column concentration data are available from https://acdisc.gesdisc.eosdis.nasa.gov/data/Aura_OMI_Level3/OMTO3e.003/. The OPAC software package can be acquired from <http://doi.org/10.5281/zenodo.6486407>. The SBDART model can be acquired from <http://doi.org/10.5281/zenodo.6486410>. The TUV model can be acquired from <http://doi.org/10.5281/zenodo.6486412>. The NCAR MM model can be acquired from <http://doi.org/10.5281/zenodo.6486414>.

Acknowledgments

This work was supported by the National Natural Science Foundation of China (Grant Nos. 42192512, 92044302, 42021004) and the Natural Science Foundation of Jiangsu Province (Grant No. BK20181100).

References

- Dickerson, R. R., Kondragunta, S., Stenichikov, G., Civerloli, K. L., Doddridge, B. G., & Holben, B. N. (1997). The impact of aerosols on solar ultraviolet radiation and photochemical smog. *Science*, 278(5339), 827–830. <https://doi.org/10.1126/science.278.5399.827>
- Ding, A. J., Huang, X., Nie, W., Sun, J. N., Kerminen, V. M., Petaja, T., et al. (2016). Enhanced haze pollution by black carbon in megacities in China. *Geophysical Research Letters*, 43(6), 2873–2879. <https://doi.org/10.1002/2016GL067745>
- Gao, J., Zhu, B., Xiao, H., Kang, H., Pan, C., Wang, D., & Wang, H. (2018). Effects of black carbon and boundary layer interaction on surface ozone in Nanjing, China. *Atmospheric Chemistry and Physics*, 18(10), 7081–7094. <https://doi.org/10.5194/acp-18-7081-2018>
- Gao, J. H., Li, Y., Zhu, B., Hu, B., Wang, L. L., & Bao, F. W. (2020). What have we missed when studying the impact of aerosols on surface ozone via changing photolysis rates? *Atmospheric Chemistry and Physics*, 20, 10831–10844. <https://doi.org/10.5194/acp-2020-140>
- Jacobson, M. Z. (1998). Studying the effects of aerosols on vertical photolysis rate coefficient and temperature profiles over an urban airshed. *Journal of Geophysical Research-Atmosphere*, 103(D9), 10593–10604. <https://doi.org/10.1029/98jd00287>
- Lei, Y. H., Letu, H., Shang, H. Z., & Shi, J. C. (2020). Cloud cover over the Tibetan plateau and eastern China: A comparison of ERA5 and ERA-interim with satellite observations. *Climate Dynamics*, 54(5–6), 2941–2957. <https://doi.org/10.1007/s00382-0-0-05149-x>
- Li, G., Bei, N., Tie, X., & Molina, L. T. (2011). Aerosol effects on the photochemistry in Mexico City during MCMA-2006/MILAGRO campaign. *Atmospheric Chemistry and Physics*, 11, 5169–5182. <https://doi.org/10.5194/acp-11-5169-2011>
- Li, J., Chen, X. S., Wang, Z. F., Du, H. Y., Yang, W. Y., Sun, Y. L., et al. (2018). Radiative and heterogeneous chemical effects of aerosol on ozone and inorganic aerosols over East Asia. *Science of the Total Environment*, 622–623, 1327–1342. <https://doi.org/10.1016/j.scitotenv.2017.12.041>
- Li, K., Jacob, D. J., Liao, H., Shen, L., Zhang, Q., & Bates, K. H. (2019). Anthropogenic drivers of 2013–2017 trends in summer surface ozone in China. *Proceedings of the National Academy of Sciences*, 116(2), 422–427. <https://doi.org/10.1073/pnas.1812168116>
- Liao, H., Yung, Y. L., & Seinfeld, J. H. (1999). Effects of aerosols on tropospheric photolysis rates in clear and cloudy atmospheres. *Journal of Geophysical Research: Atmosphere*, 104(D19), 23697–23707. <https://doi.org/10.1029/1999JD900409>
- Liu, X. F., Wang, N., Lyu, X. P., Zeren, Y. Z., Jiang, F., Wang, X. M., et al. (2021). Photochemistry of ozone pollution in autumn in pearl river estuary, south China. *Science of the Total Environment*, 754, 141812. <https://doi.org/10.1016/j.scitotenv.2020.141812>
- Lu, Q., Liu, C., Zeng, C., Zhao, D. L., Li, J., Lu, C., et al. (2020). Atmospheric heating rate due to black carbon aerosols: Uncertainties and impact factors. *Atmospheric Research*, 240, 104891. <https://doi.org/10.1016/j.atmosres.20.104891>
- Lu, X., Zhang, L., Wang, X., Gao, M., Li, K., Zhang, Y., et al. (2020). Rapid increases in warm-season surface ozone and resulting health impact in China since 2013. *Environmental Science and Technology Letters*, 7(4), 240–247. <https://doi.org/10.1021/acs.estlett.0c00171>
- Macintyre, H. L., & Evans, M. J. (2011). Parameterization and impact of aerosol uptake of HO₂ on a global tropospheric model. *Atmospheric Chemistry and Physics*, 11(21), 10965–10974. <https://doi.org/10.5194/acp-11-10965-2011>
- Maryam, G., Abbasali, A. B., & Khan, A. (2021). The interaction of ozone and aerosol in a semi-arid region in the Middle East: Ozone formation and radiative forcing implications. *Atmospheric Environment*, 245, 118015. <https://doi.org/10.1016/j.atmosenv.2020.118015>
- Qu, Y. W., Wang, T. J., Wu, H., Shu, L., Li, M. M., Chen, P. L., et al. (2020). Vertical structure and interaction of ozone and fine particulate matter in spring at Nanjing, China: The role of aerosol's radiation feedback. *Atmospheric Environment*, 222, 117162. <https://doi.org/10.1016/j.atmosenv.2019.117162>
- Seinfeld, J. H. (1989). Urban air pollution: State of the science. *Science*, 243(4892), 745–752. <https://doi.org/10.1126/science.243.4892.745>
- Tie, X. X., Madronich, S., Walters, S., Edwards, D. P., Ginoux, P., Mahowald, N., et al. (2005). Assessment of the global impact of aerosols on tropospheric oxidants. *Journal of Geophysical Research-Atmosphere*, 110(D3), D03204. <https://doi.org/10.1029/2004JD005359>
- Villa, T., Salimi, F., Morton, K., Morawska, L., & Gonzalez, F. (2016). Development and validation of a UAV based system for air pollution measurements. *Sensors*, 16(12), 2202. <https://doi.org/10.3390/s16122202>
- Wang, J., Allen, D. J., Pickering, K. E., Li, Z. Q., & He, H. (2016). Impact of aerosol direct effect on East Asian air quality during the EAST-AIRE campaign. *Journal of Geophysical Research-Atmosphere*, 121(11), 6534–6554. <https://doi.org/10.1002/2016JD025108>
- Zhang, M., Ma, Y., Gong, W., Liu, B., Shi, Y., & Chen, Z. (2018). Aerosol optical properties and radiative effects: Assessment of urban aerosols in central China using 10-year observations. *Atmospheric Environment*, 182, 275–285. <https://doi.org/10.1016/j.atmosenv.2018.03.040>
- Zhang, Y. Q., Shindell, D., Seltzer, K., Shen, L., Lamarque, J. F., Zhang, Q., et al. (2021). Impacts of emission changes in China from 2010 to 2017 on domestic and intercontinental air quality and health effect. *Atmospheric Chemistry and Physics*, 21(20), 16051–16065. <https://doi.org/10.5194/acp-21-16051-2021>
- Zhu, B., Zhi, L. R., Lu, W., Gao, J. H., & Hou, X. W. (2021). Observational analysis and numerical simulation of effect of black carbon on ozone in Nanjing and its surrounding areas. *Transactions of Atmospheric Sciences*, 44, 626–635. <https://doi.org/10.13878/j.cnki.dqkxxb.20190415002>
- Zhu, J., Chen, L., Liao, H., Yang, H., Yang, Y., & Yue, X. (2021). Enhanced PM_{2.5} decreases and O₃ increases in China during COVID-19 lockdown by aerosol-radiation feedback. *Geophysical Research Letters*, 48(2), e2020GL090260. <https://doi.org/10.1029/2020GL090260>

References From the Supporting Information

- An, J. L., Lv, H., Xue, M., Zhang, Z. F., Hu, B., Wang, J. X., & Zhu, B. (2021). Analysis of the effect of optical properties of black carbon on ozone in an urban environment at the Yangtze River Delta, China. *Advances in Atmospheric Sciences*, 38(7), 1153–1164. <https://doi.org/10.1007/s00376-021-0367-9>
- Han, S. Q., Hao, T. Y., Zhang, Y. F., Liu, J. L., Li, P. Y., Cai, Z. Y., et al. (2018). Vertical observation and analysis on rapid formation and evolutionary mechanisms of a prolonged haze episode over central-eastern China. *Science of the Total Environment*, 616–617, 135–146. <https://doi.org/10.1016/j.scitotenv.2017.10.278>
- Hansen, A. D. A., Rosen, H., & Novakov, T. (1984). The aethalometer—An instrument for the real-time measurement of optical absorption by aerosol particles. *Science of the Total Environment*, 36, 191–196. [https://doi.org/10.1016/0048-9697\(84\)90265-1](https://doi.org/10.1016/0048-9697(84)90265-1)
- Hess, M., Koepke, P., & Schultz, I. (1998). Optical properties of aerosols and clouds: The software package OPAC. *Bulletin of the American Meteorological Society*, 79(5), 831–844. [https://doi.org/10.1175/1520-0477\(1998\)079<0831:opoaac>2.0.co;2](https://doi.org/10.1175/1520-0477(1998)079<0831:opoaac>2.0.co;2)
- Madronich, S., & Flocke, S. (1999). The role of solar radiation in atmospheric chemistry. In *Boule P. Environmental photochemistry* (pp. 14–15). Springer. https://doi.org/10.1007/978-3-540-69044-3_1
- Pant, P., Habib, G., Marshall, J. D., & Peltier, R. E. (2017). PM_{2.5} exposure in highly polluted cities: A case study from New Delhi, India. *Environmental Research*, 156, 167–174. <https://doi.org/10.1016/j.envres.2017.03.024>
- Ricchiazzi, P., Yang, S., Gautier, C., & Sowle, D. (1998). SBDART: A research and teaching software tool for plane-parallel radiative transfer in the Earth's atmosphere. *Bulletin of the American Meteorological Society*, 79(10), 2101–2114. [https://doi.org/10.1175/1520-0477\(1998\)0792.0.CO;2](https://doi.org/10.1175/1520-0477(1998)0792.0.CO;2)
- Tripathi, S. N., Srivastava, A. K., Dey, S., Satheesh, S. K., & Krishnamoorthy, K. (2007). The vertical profile of atmospheric heating rate of black carbon aerosols at Kanpur in northern India. *Atmospheric Environment*, 41(32), 6909–6915. <https://doi.org/10.1016/j.atmosenv.2007.06.032>
- Weingartner, E., Saathoff, H., Schnaiter, M., Streit, N., Bitnar, B., & Baltensperger, U. (2003). Absorption of light by soot particles: Determination of the absorption coefficient by means of aethalometers. *Journal of Aerosol Science*, 34(10), 1445–1463. [https://doi.org/10.1016/S0021-8502\(03\)00359-8](https://doi.org/10.1016/S0021-8502(03)00359-8)